

# Form Factor Effects in the Direct Detection of Isospin-Violating Dark Matter

Hao Zheng<sup>1</sup>, Zhen Zhang<sup>1</sup> and Lie-Wen Chen<sup>\*1,2</sup>

<sup>1</sup>*Department of Physics and Astronomy and Shanghai Key Laboratory for Particle Physics and Cosmology, Shanghai Jiao Tong University, Shanghai 200240, China*

<sup>2</sup>*Center of Theoretical Nuclear Physics, National Laboratory of Heavy Ion Accelerator, Lanzhou 730000, China*

(Dated: June 10, 2022)

Isospin-violating dark matter (IVDM) provides a possible mechanism to ameliorate the tension among recent direct detection experiments. For IVDM, we demonstrate that the results of direct detection experiments based on neutron-rich target nuclei may depend strongly on the density dependence of the symmetry energy which is presently largely unknown and controls the neutron skin thickness that reflects the relative difference of neutron and proton form factors in the neutron-rich nuclei. In particular, using the neutron and proton form factors obtained from Skyrme-Hartree-Fock calculations by varying the symmetry energy within the uncertainty region set by the latest model-independent measurement of the neutron skin thickness of <sup>208</sup>Pb from PREX experiment at JLab, we find that, for IVDM with neutron-to-proton coupling ratio fixed to  $f_n/f_p = -0.7$ , the form factor effect may enhance the sensitivity of Xe-based detectors (e.g., XENON100 and LUX) to the DM-proton cross section by a factor of 3 in the DM mass region constrained by CMDS-II(Si) and even by more than an order of magnitude for heavy DM with mass larger than 80 GeV, compared with the results using the empirical Helm form factor. Our results further indicate that the form factor effect can significantly modify the recoil spectrum of Xe-based detectors for heavy IVDM with  $f_n/f_p = -0.7$ .

## I. INTRODUCTION

The possible existence of dark matter (DM) is one of the most intriguing aspects of modern particle physics, astrophysics and cosmology. In order to survey the nature of DM, a number of observations and experiments have been conducted or are underway around the world. The most recent cosmological results based on *Planck* measurements of the cosmic microwave background (CMB) temperature and lensing-potential power spectra indicate that DM comprises about 27% of the energy density of the Universe which also includes about 5% baryon matter and about 68% dark energy [1]. Many theories beyond the Standard Model of particle physics predict natural candidates for DM, e.g., the weakly interacting massive particles (WIMPs) which are a class of hypothetical stable neutral particles with a huge range in masses from 1 GeV to 100 TeV and interaction cross sections with normal matter (proton) from  $10^{-40}$  to  $10^{-50}$  cm<sup>2</sup> [2, 3]. In terrestrial laboratory, DM might be directly detected through their elastic scattering off nuclei in particle detectors [4]. A number of underground DM direct detection experiments have been performed, and among them an excess of events over the expected background has been observed by CoGeNT [5], DAMA [6], CRESSTII [7] as well as in the recent results presented by the CDMS-II(Si) collaboration [8, 9]. However, these results are in strong tension with the constraints set by some other experimental groups like XENON100 [10, 11], LUX [12] and SuperCDMS(Ge) [13], leaving a confusing situation for the community. This has led to a number of attempts trying to explain the discrepancy by considering atomic uncertainties [14] or different mechanisms that deviate from standard assumptions about DM interactions or its astrophysical distributions [15–18].

Isospin-Violating Dark Matter (IVDM) provides a very promising mechanism to reconcile the tension among different experiments [19–26]. Within the IVDM framework, DM is assumed to couple differently with protons and neutrons, and this assumption of the isospin violation has been supported by a number of theoretical works [27–32] based on the particle physics point of view. Many parameters need to be specified in the standard method of analyzing DM direct detection experiments [33] and recently Frandsen *et al.* [34] presented a systematic discussion on the possible ways to ameliorate the tension among different experiments. They found that the tension between the CDMS-II(Si) results and the XENON100 bounds is independent of the astrophysical uncertainties concerning the DM halo and any momentum- and velocity-dependence of the cross section in particle physics, but it can be largely ameliorated or even resolved within the framework of IVDM.

Besides the uncertainties in astrophysics and particle physics concerning the interaction of a DM particle scattering off a single nucleon mentioned above, the uncertainties in nuclear physics describing how the struck nucleon is distributed inside the nucleus may also play an important role in interpreting DM signals. This is because in DM direct detection experiments, the nuclear form factors are generally applied to describe the DM-nucleus cross section

---

\* Corresponding author (email: lwchen@sjtu.edu.cn)

and the bounds on DM-nucleon cross section are then obtained accordingly. In particular, the empirical Helm form factor extracted from nuclear charge distributions [35, 36] has been commonly adopted in current direct detection experiments. However, the DM-nucleus interaction should be in principle described by using the form factors of both proton and neutron distributions in the nuclei rather than the charge distributions since the DM particles actually interact with the protons and neutrons in the nuclei. Within the framework of relativistic mean field (RMF) model, Chen *et al.* [37] derived the nuclear form factor for the spin-independent scattering between the WIMPs and nucleus, and they found that the results can deviate from the empirical Helm form factor by 15% to 25% in a large range of recoil spectrum of  $0 \sim 100$  keV. A recent work by Co' *et al.* [38] suggests that the use of different distributions for protons and neutrons instead of the commonly used empirical charge distributions for a target nucleus could be important in interpreting DM signals, especially if IVDM is considered.

For stable nuclei, the proton distribution can be well determined from the charge distribution which can be accurately measured with electron scattering [39–41]. In contrast, the neutron distribution is usually determined from hadron scattering experiments and the results are generally highly model dependent due to the unclear non-perturbative strong interaction [42]. Recently, the Lead Radius Experiment (PREX) collaboration at Jefferson Laboratory (JLab) published their results on the measurement of the parity-violating cross section asymmetry in the elastic scattering of polarized electrons from  $^{208}\text{Pb}$  [42], which provides a model-independent determination of the neutron density distributions in  $^{208}\text{Pb}$ . The PREX measurement leads to a value of  $\sqrt{\langle r_n^2 \rangle} = 5.78_{-0.18}^{+0.16}$  fm for the rms radius of the neutron distributions for  $^{208}\text{Pb}$ , implying a large neutron skin thickness, i.e.,  $\Delta r_{\text{np}} = \sqrt{\langle r_n^2 \rangle} - \sqrt{\langle r_p^2 \rangle} = 0.33_{-0.18}^{+0.16}$  fm by assuming a point-proton rms radius of 5.45 fm [43]. One can see that the obtained value of  $\Delta r_{\text{np}}$  has a large error, indicating a large uncertainty of the neutron distribution relative to the proton distribution in  $^{208}\text{Pb}$ .

Theoretically, it has been established [44, 45] that the  $\Delta r_{\text{np}}$  is intimately related to the nuclear matter symmetry energy which characterizes the isospin dependent part of the equation of state (EOS) of asymmetric nuclear matter (ANM) [46]. In particular, it has been shown recently that the  $\Delta r_{\text{np}}$  of heavy nuclei is uniquely determined by the density slope  $L(\rho_c)$  of the symmetry energy at a subsaturation cross density  $\rho_c \approx 0.11 \text{ fm}^{-3}$  [47]. These features imply that the uncertainties of  $\Delta r_{\text{np}}$ , especially the neutron distributions, predicted by various nuclear models are essentially due to our poor knowledge about the symmetry energy. The symmetry energy is of critical importance for understanding not only the structure and reaction of radioactive nuclei, but also a number of interesting issues in astrophysics, such as the structure of neutron stars and the mechanism of supernova explosions, and has become a hot topic in current research frontiers of nuclear physics and astrophysics [48]. The determination of the symmetry energy provides a strong motivation for studying isospin-dependent phenomena with radioactive nuclei at a number of new/planning rare isotope beam facilities around the world, such as CSR/Lanzhou and BRIF-II/Beijing in China, RIBF/RIKEN in Japan, SPIRAL2/GANIL in France, FAIR/GSI in Germany, SPES/LNL in Italy, RAON in Korea, and FRIB/NSCL and T-REX/TAMU in USA. In this work, using the proton and neutron form factors obtained from Skyrme-Hartree-Fock calculations by varying the symmetry energy slope parameter  $L(\rho_c)$  within the uncertainty region set by the PREX experiment, we investigate the form factor effects in the direct detection of dark matter.

This article is organized as follows. We briefly introduce in Sec. II the theoretical models and methods used in the present work, and then present the results and discussions in Sec. III. Finally, a conclusion is given in Sec. IV.

## II. MODELS AND METHODS

### A. The symmetry energy and Skyrme-Hartree-Fock approach

The EOS of isospin asymmetric nuclear matter, defined by its binding energy per nucleon, can be well approximated by

$$E(\rho, \delta) = E_0(\rho) + E_{\text{sym}}(\rho)\delta^2 + \mathcal{O}(\delta^4), \quad (1)$$

in terms of baryon density  $\rho = \rho_p + \rho_n$  and isospin asymmetry  $\delta = (\rho_n - \rho_p)/\rho$  with  $\rho_p$  and  $\rho_n$  denoting the proton and neutron densities, respectively.  $E_0(\rho) = E(\rho, \delta = 0)$  corresponds to the EOS of symmetric nuclear matter, and the nuclear symmetry energy can be expressed as

$$E_{\text{sym}}(\rho) = \frac{1}{2!} \left. \frac{\partial^2 E(\rho, \delta)}{\partial \delta^2} \right|_{\delta=0}. \quad (2)$$

There are no odd-order  $\delta$  terms in Eq. (1) due to the exchange symmetry between protons and neutrons (isospin symmetry) in nuclear matter. Neglecting the contribution from higher-order terms in Eq. (1) leads to the well-known

empirical parabolic law for EOS of ANM, which has been verified by all many-body theories to date, at least for densities up to moderate values [46].

Furthermore, around a reference density  $\rho_r$ , the symmetry energy  $E_{\text{sym}}(\rho)$  can be expanded as

$$E_{\text{sym}}(\rho) = E_{\text{sym}}(\rho_r) + \frac{L(\rho_r)}{3} \left( \frac{\rho - \rho_r}{\rho_r} \right) + \mathcal{O} \left( \frac{\rho - \rho_r}{\rho_r} \right)^2, \quad (3)$$

with

$$L(\rho_r) = 3\rho_r \left. \frac{\partial E_{\text{sym}}(\rho)}{\partial \rho} \right|_{\rho=\rho_r}. \quad (4)$$

The slope parameter  $L(\rho_r)$  characterizes the density dependence of symmetry energy around  $\rho_r$ . It has been shown [47] that the neutron skin thickness  $\Delta r_{\text{np}}$  of heavy nuclei is uniquely fixed by the density slope  $L(\rho_c)$  at a subsaturation cross density  $\rho_c \approx 0.11 \text{fm}^{-3}$  which roughly corresponds to the average density of the nuclei.

For the calculations of finite nuclei, we use in the present work the standard Skyrme-Hartree-Fock (SHF) approach in which the nuclear effective interaction is taken to have a zero-range, density- and momentum-dependent form, i.e. [49],

$$\begin{aligned} V_{12}(\mathbf{R}, \mathbf{r}) = & t_0(1 + x_0 P_\sigma) \delta(\mathbf{r}) \\ & + \frac{1}{6} t_3(1 + x_3 P_\sigma) \rho^\sigma(\mathbf{R}) \delta(\mathbf{r}) \\ & + \frac{1}{2} t_1(1 + x_1 P_\sigma) (K'^2 \delta(\mathbf{r}) + \delta(\mathbf{r}) K^2) \\ & + t_2(1 + x_2 P_\sigma) \mathbf{K}' \cdot \delta(\mathbf{r}) \mathbf{K} \\ & + iW_0(\sigma_1 + \sigma_2) \cdot [\mathbf{K}' \times \delta(\mathbf{r}) \mathbf{K}], \end{aligned} \quad (5)$$

with  $\mathbf{r} = \mathbf{r}_1 - \mathbf{r}_2$  and  $\mathbf{R} = (\mathbf{r}_1 + \mathbf{r}_2)/2$ . In the above expression, the relative momentum operators  $\mathbf{K} = (\nabla_1 - \nabla_2)/2i$  and  $\mathbf{K}' = -(\nabla_1 - \nabla_2)/2i$  act on the wave function on the right and left, respectively. The quantities  $P_\sigma$  and  $\sigma_i$  denote, respectively, the spin exchange operator and Pauli spin matrices.

The Skyrme interaction in Eq. (5) includes totally 10 parameters, i.e., the 9 Skyrme interaction parameters  $\sigma$ ,  $t_0 - t_3$ ,  $x_0 - x_3$ , and the spin-orbit coupling constant  $W_0$ . This standard SHF approach has been shown to be very successful in describing the structure of finite nuclei, especially the global properties such as binding energies and charge radii [49–51]. Instead of using directly the 9 Skyrme interaction parameters, we can express them explicitly in terms of 9 macroscopic quantities, i.e.,  $\rho_0$ ,  $E_0(\rho_0)$ , the incompressibility  $K_0$ , the isoscalar effective mass  $m_{s,0}^*$ , the isovector effective mass  $m_{v,0}^*$ ,  $E_{\text{sym}}(\rho_r)$ ,  $L(\rho_r)$ ,  $G_S$ , and  $G_V$ . The  $G_S$  and  $G_V$  are respectively the gradient and symmetry-gradient coefficients in the surface interaction part of the binding energies for finite nuclei which is defined as

$$E_{\text{grad}} = G_S (\nabla \rho)^2 / (2\rho) - G_V [\nabla(\rho_n - \rho_p)]^2 / (2\rho). \quad (6)$$

Then, by varying individually these macroscopic quantities within their known ranges, one can examine more transparently the correlation of nuclear matter properties with each individual macroscopic quantity. Recently, this correlation analysis method has been successfully applied to study the neutron skin [47, 52] and giant monopole resonance of finite nuclei [53], the higher-order bulk characteristic parameters of ANM [54], and the relationship between the nuclear matter symmetry energy and the symmetry energy coefficient in nuclear mass formula [55]. In the present work, we use the 9 macroscopic quantities instead of using directly the 9 Skyrme interaction parameters. Especially, we study the symmetry energy effects by varying the  $L(\rho_c)$  value while keeping the other macroscopic quantities unchanged.

## B. Method of Analyzing DM Direct Detection Experiments

In this work, we use the standard method of analyzing DM direct detection experiments [33, 34]. The spin-independent differential event rate of nuclear recoils with a recoil energy of  $E_R$ , occurring in a detector due to an elastic collision between a target nucleus of mass  $m_N^A$  and a DM particle of mass  $m_\chi$ , can be expressed as

$$\frac{dR^A}{dE_R} = \frac{\rho_\chi N_T^A}{m_N^A m_\chi} \int_{v_{\text{min}}}^{v_E + v_{\text{esc}}} v_\chi f(\mathbf{v}_\chi + \mathbf{v}_E) \frac{d\sigma_{\text{P}}}{dE_R} A^2 |F_A(q)|^2 d^3 v_\chi, \quad (7)$$

where  $A$  represents the mass number of the target nucleus and  $N_T^A$  is the number of target nucleus per unit mass in the detector,  $\rho_\chi$  is the local halo DM density,  $f(v_\chi)$  is the local DM velocity distribution evaluated in the Galactic rest frame with  $v_\chi = |\mathbf{v}_\chi|$ ,  $\mathbf{v}_E$  is Earth velocity in the Galactic rest frame, and  $v_{\text{esc}}$  is the Galactic escape velocity [56, 57].  $\frac{d\sigma_p}{dE_R}$  and  $F_A(q)$  denote, respectively, the spin-independent differential DM-proton scattering cross-section and the effective form factors, and they will be detailed below. The  $q = (2m_N^A E_R)^{1/2}$  is the momentum transfer between the DM particle and the struck nucleus. The lower limit  $v_{\text{min}}$  of the integration in Eq. (7) corresponds to the smallest DM velocity that can give a recoil energy of  $E_R$ , i.e.,

$$v_{\text{min}}(E_R) = \sqrt{\frac{m_N^A E_R}{2\mu_A^2}}, \quad (8)$$

where  $\mu_A = m_N^A m_\chi / (m_N^A + m_\chi)$  is the DM-nucleus reduced mass. The predicted normalized recoil spectrum can thus be expressed as

$$f_s(E_R) = \frac{\sum_A \eta_A \frac{dR^A}{dE_R}}{\sum_A \eta_A \int \frac{dR^A}{dE_R} dE_R}, \quad (9)$$

where  $\eta_A$  is the natural abundance of the isotope with mass number  $A$  for the target element.

The total event rate  $R_{\text{ex}}$  expected in an energy range  $[E_1, E_2]$  in a detector consisting of compound targets with finite detector energy resolution, usually characterized by the unit of one event  $kg^{-1} d^{-1}$ , can be written as [34]

$$R_{\text{ex}} = \sum_A \eta_A \int dE_R \epsilon(E_R) \text{Res}(E_R, E_1, E_2) \frac{dR^A}{dE_R}, \quad (10)$$

where  $\epsilon(E_R)$  and  $\text{Res}(E_R, E_1, E_2)$  are the detector acceptance and the detector response function, respectively. The  $E_R$  integration region is determined by the cuts in the experiments.

It is convenient, and usually adequate, to describe the matter distributions of a finite nucleus by a form factor,  $F$ , in analyzing DM direct detection experiments [33]. In the first-order Born approximation, the form factors of spherical nuclei are the Fourier transforms of the proton and neutron density distributions, i.e.,

$$F_A^{\text{p,n}}(q) = \int \rho_A^{\text{p,n}}(\mathbf{r}) e^{i\mathbf{q}\cdot\mathbf{r}} d^3r = \frac{4\pi}{q} \int_0^\infty r \sin(qr) \rho_A^{\text{p,n}}(r) dr, \quad (11)$$

where the index p (n) denotes protons (neutrons). The density distributions,  $\rho_A^{\text{p,n}}$ , for spherical nuclei can be obtained by using a mean-field approach [58], e.g., the SHF approach as we discussed above.

We further define the so-called effective form factors in Eq. (7) in terms of  $F_A^{\text{p,n}}$  as

$$|F_A(q)|^2 = \frac{1}{A^2} |ZF_A^{\text{p}}(q) + g_{\text{np}} N F_A^{\text{n}}(q)|^2, \quad (12)$$

where  $Z$  ( $N$ ) is the proton (neutron) number of the target nucleus,  $A=Z+N$ , and  $g_{\text{np}} = f_n/f_p$  is the isospin-violation factor with  $f_n$  and  $f_p$  denoting the effective coupling of DM to neutrons and protons, respectively. The spin-independent differential DM-proton scattering cross-section can then be expressed as [34]

$$\frac{d\sigma_p}{dE_R} = \frac{m_N^A \sigma_p}{2\mu_{\text{p}\chi}^2 v_\chi^2}, \quad (13)$$

where  $\mu_{\text{p}\chi}$  is the reduced DM-proton mass, and  $\sigma_p$  is the elastic DM-proton cross-section at zero momentum transfer ( $q = 0$ ). Integrating the differential event rate in Eq. (7) with respect to  $E_R$ , i.e., Eq. (10), one can relate the expected number of scattering events in a direct detection experiment with the DM-proton cross-section  $\sigma_p$ . Furthermore, by adopting, e.g., a profile likelihood analysis proposed by the XENON100 collaboration [59] or the maximum gap method introduced by Yellin [60] *et al.*, one can constrain the elastic DM-proton cross-section  $\sigma_p$  in the  $m_\chi$ - $\sigma$  plane with specific confidence level.

However, in experiments usually reported is the DM-nucleon cross section  $\sigma_N$ , rather than  $\sigma_p$ .  $\sigma_N$  is an effective cross section by assuming that the DM particle couples with protons and neutrons equally (i.e.,  $g_{\text{np}} = 1$ ) and the protons and neutrons have identical form factor which is in practice commonly taken as the empirical charge form factor parameterized by Helm [35]. Obviously, the DM-proton cross section  $\sigma_p$  is generally different from the DM-nucleon cross section  $\sigma_N$ , but they can be related to each other by the so-called degradation factor  $D_p$  defined as [23]

$$D_p \equiv \frac{\sigma_N}{\sigma_p} = \frac{\sum_A \eta_A N_T^A A^2 \int \epsilon(E_R) \text{Res}(E_R, E_1, E_2) k(E_R, m_\chi) |F_A(E_R)|^2 dE_R}{\sum_A \eta_A N_T^A A^2 \int \epsilon(E_R) \text{Res}(E_R, E_1, E_2) k(E_R, m_\chi) |F_A^{\text{Helm}}(E_R)|^2 dE_R}, \quad (14)$$

with

$$k(E_R, m_\chi) = \int_{v_{\min}(E_R, m_\chi)}^{v_E + v_{\text{esc}}} f(\mathbf{v}_\chi + \mathbf{v}_E) / v_\chi d^3 v_\chi, \quad (15)$$

In Eq. (14),  $F_A^{\text{Helm}}$  is the Helm form factor which is obtained by using a charge density with a Gaussian surface distribution and has the following simple analytical expression

$$F_A^{\text{Helm}}(q) = 3 \frac{j_1(qr_N)}{qr_N} \times e^{-(qs)^2/2}, \quad (16)$$

where  $j_1$  is the first-order spherical Bessel function,  $r_N$  is an effective nuclear radius and  $s$  is a measure of the nuclear skin thickness. For  $r_N$  and  $s$ , the following standard parametrization has been used [33]

$$r_N^2 = c^2 + \frac{7}{3} \pi^2 a^2 - 5s^2, \quad (17)$$

$$c \approx 1.23A^{1/3} - 0.60 \text{ fm}, \quad (18)$$

$$a \approx 0.52 \text{ fm}, \quad (19)$$

$$s \approx 0.9 \text{ fm}. \quad (20)$$

In Eq. (14), it has been assumed that the variations of  $g_{\text{np}}$  and form factors do not change the shape of recoil spectra  $f_s(E_R)$  in Eq. (9). In this case, varying  $g_{\text{np}}$  and form factors does not change the event distributions but simply modifies the expected number of total events,  $R_{\text{ex}}$  in Eq. (10), for a given cross section. In general cases with different  $g_{\text{np}}$  and nuclear form factors, since  $R_{\text{ex}} \propto \sigma_p$ , we can simply rescale the corresponding cross sections according to the degradation factor as  $\sigma_p = \sigma_N / D_p$  to keep the likelihood function (the maximum gap) in a profile likelihood analysis (the maximum gap method) unchanged. However, if the recoil spectrum changes significantly, the degradation factor in Eq. (14) should be modified according to the following identity

$$D_p = D_p^0 \times \frac{R_{\text{ex}}(\sigma_N^{\text{up}})}{R_{\text{ex}}(\sigma_p^{\text{up}})}, \quad (21)$$

where  $D_p^0$  denotes the degradation factor defined in Eq. (14),  $R_{\text{ex}}(\sigma_p^{\text{up}})$  and  $R_{\text{ex}}(\sigma_N^{\text{up}})$  are the number of expected events with  $\sigma_p^{\text{up}}$  and  $\sigma_N^{\text{up}}$  being the upper limits of the DM-proton and DM-nucleon cross sections with certain confidence level. We estimate  $R_{\text{ex}}(\sigma_p^{\text{up}})$  and  $R_{\text{ex}}(\sigma_N^{\text{up}})$  by using the ‘‘maximum gap method’’ [60] in this work. In this way, one can thus study the isospin-violating effects and the form factor effects simultaneously in analyzing the DM signals.

### III. RESULTS AND DISCUSSIONS

#### A. Symmetry energy effects on nuclear form factors

As mentioned above, the neutron skin thickness of heavy nuclei is uniquely determined by the symmetry energy density slope parameter  $L(\rho_c)$  at a subsaturation cross density  $\rho_c \approx 0.11 \text{ fm}^{-3}$  [47]. Therefore, the  $L(\rho_c)$  parameter controls the relative difference between the neutron and proton distributions (and thus the neutron and proton form factors) in the nuclei. In the present work, we investigate the form factor effects by varying the  $L(\rho_c)$  parameter in the SHF calculations to fit the model-independent result of  $\Delta r_{\text{np}} = 0.33_{-0.18}^{+0.16} \text{ fm}$  for  $^{208}\text{Pb}$  from the recent PREX experiment at JLab.

Shown in Fig. 1 is the  $\Delta r_{\text{np}}$  of  $^{132}\text{Xe}$  as a function of that of  $^{208}\text{Pb}$  in SHF calculations with the Skyrme interaction MSL1 [47] by varying  $L(\rho_c)$  while keeping the other 8 macroscopic quantities and the spin-orbit coupling constant  $W_0$  fixed at their default values in the MSL1 interaction, namely,  $\rho_0 = 0.1586 \text{ fm}^{-3}$ ,  $E_0(\rho_0) = -15.998 \text{ MeV}$ , the incompressibility  $K_0 = 235.12 \text{ MeV}$ , the isoscalar effective mass  $m_{s,0}^* = 0.806m$ , the isovector effective mass  $m_{v,0}^* = 0.706m$ ,  $E_{\text{sym}}(\rho_c) = 26.67 \text{ MeV}$ ,  $G_S = 126.69 \text{ MeV} \cdot \text{fm}^5$ ,  $G_V = 68.74 \text{ MeV} \cdot \text{fm}^5$ , and  $W_0 = 113.62 \text{ MeV} \cdot \text{fm}^5$ . The MSL1 interaction has been obtained by fitting a number of experimental data of finite nuclei, including the binding energy, the charge rms radius, the neutron  $3p_{1/2} - 3p_{3/2}$  energy level splitting in  $^{208}\text{Pb}$ , isotope binding energy difference, and neutron skin data of Sn isotopes. For comparison, we also include in Fig. 1 the results from SHF calculations with 43 other Skyrme interactions (BSk1, BSk4, BSk5, BSk7, BSk10, BSk14, BS15, Dutta, E-fit, Esigma-fit, Gsigma-fit, KDE, KDE0, MSL0, RATP, Rsigma-fit, SGI, SGII, SK255, SK272, SKa, SkI1, SkI2, SkI5, SKM, SkMP, SKM\*, SKT1, SKT4, SKT5, SKT6, Skz0, Skz1, Skz2, Skz3, Skz4, Skz-1, SLy4, SLy5, SLy9, Z-fit,



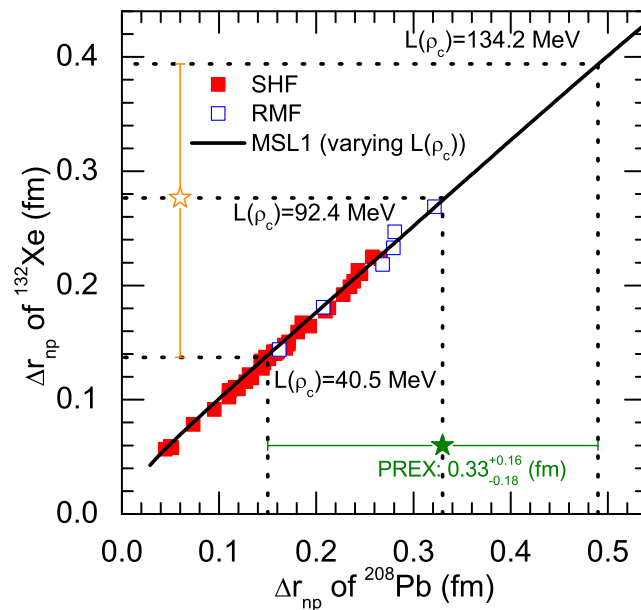


Figure 1: (Color online) Neutron skin thickness for  $^{132}\text{Xe}$  vs. that for  $^{208}\text{Pb}$  predicted by mean-field models with different interactions. Constraints set by PREX measurement [42] are also shown.

Zsigma-fit, and ZsigmaS-fit) and RMF calculations with 6 different interaction parameter sets (FSU, IUFSU, TM1, PK1, NL3, and NL1). The references of these Skyrme and RMF interactions can be found in Refs. [61–63]. We have selected these interactions in such a way that their  $L(\rho_c)$  values scatter in large region and are not close to each other. One can see clearly a nice model-independent linear correlation between the neutron skin thicknesses of  $^{208}\text{Pb}$  and  $^{132}\text{Xe}$  within the non-relativistic and relativistic models with different interactions. In addition, although there are few interactions that predict a  $\Delta r_{\text{np}}$  of  $^{208}\text{Pb}$  larger than 0.33 fm measured by the model-independent PREX experiment, one can easily obtain a large  $\Delta r_{\text{np}}$  of  $^{208}\text{Pb}$  by increasing the  $L(\rho_c)$  value in the MSL1 interaction. In particular, we find a value of  $L(\rho_c) = 92.4^{+41.8}_{-51.9}$  MeV in the MSL1 interaction predicts  $\Delta r_{\text{np}} = 0.33^{+0.16}_{-0.18}$  fm for  $^{208}\text{Pb}$  and  $\Delta r_{\text{np}} = 0.28^{+0.12}_{-0.14}$  fm for  $^{132}\text{Xe}$ . Therefore, we use  $L(\rho_c) = 40.5$  MeV, 92.4 MeV and 134.2 MeV in the MSL1 interaction, denoted as Lc40, Lc92 and Lc134, respectively, to study the symmetry energy and form factor effects in the present work. We would like to point out that the large neutron skin thickness for  $^{208}\text{Pb}$  measured by the PREX experiment can also be explained within the RMF model [64].

To test the Skyrme interaction parameter sets Lc40, Lc92, and Lc134, we calculate the binding energies and charge rms radii for a number of closed-shell or semi-closed-shell nuclei, i.e.,  $^{16}\text{O}$ ,  $^{40}\text{Ca}$ ,  $^{48}\text{Ca}$ ,  $^{56}\text{Ni}$ ,  $^{90}\text{Zr}$ ,  $^{100}\text{Sn}$ ,  $^{132}\text{Sn}$ , and  $^{208}\text{Pb}$ , as well as the nuclei  $^{28}\text{Si}$ ,  $^{74}\text{Ge}$ , and  $^{132}\text{Xe}$ . The elements Si, Ge and Xe are widely used as targets in the DM direct detection experiments. For Si and Ge, their natural abundances are mostly dominated by their isotopes of  $^{28}\text{Si}$  and  $^{74}\text{Ge}$ , respectively. For Xe, however, it has several isotopes with comparable natural abundances and here we just select one of them, i.e.  $^{132}\text{Xe}$ , as an example to show its properties. Fig. 2 shows the relative deviation of the binding energies and charge rms radii of these nuclei from those measured in experiments [65–67]. It is seen that the interactions Lc40 and Lc92 can describe the experimental data very well (the deviations are within about  $\pm 1\%$ ) except for the light nucleus  $^{16}\text{O}$  for which the deviation of charge rms radius is about 2.6%. It is interesting to see that, the interaction Lc134, which predicts a very strong density dependence of the symmetry energy at  $\rho_c$  and gives a very large neutron skin thickness of  $\Delta r_{\text{np}} = 0.49$  fm for  $^{208}\text{Pb}$  (the upper limit of the PREX measurement), still can give a reasonable description of the experimental data (the deviations are within about  $\pm 2\%$  as indicated by bands in Fig. 2) except the nucleus  $^{132}\text{Sn}$  for which the deviation of charge rms radius (binding energy) reaches about  $-2.6\%$  ( $3.7\%$ ) and for the light nucleus  $^{16}\text{O}$  the deviation of charge rms radius is still about 2.6%. These results are remarkable as Lc40, Lc92 and Lc134 are not obtained from fitting measured binding energies and charge rms radii of finite nuclei as in usual Skyrme parametrization. It should be pointed out that our main motivation for introducing the interactions Lc40, Lc92 and Lc134 is not to construct new Skyrme interaction parameter sets to describe data, but to use them as references to study the form factor effects in the following.

To investigate the symmetry energy effects on the proton and neutron form factors in finite nuclei, we plot in Fig. 3 the proton (upper panels) and neutron (lower panels) form factors as functions of momentum transfer  $q$  for  $^{28}\text{Si}$  (left panels) and  $^{132}\text{Xe}$  (right panels) from SHF calculations with Lc40, Lc92 and Lc134. For comparison, the results are

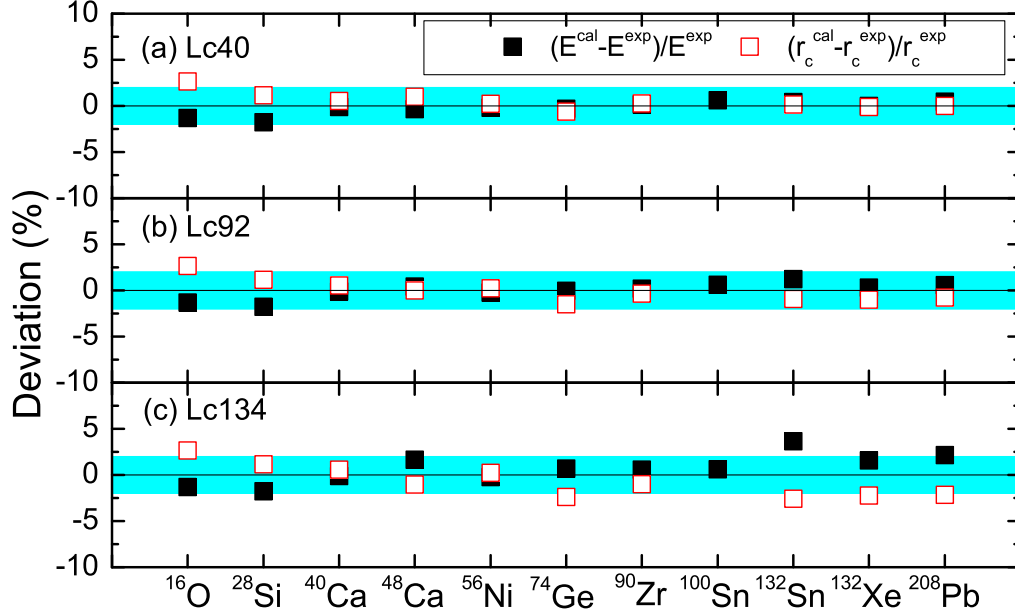


Figure 2: (Color online) Deviations of the binding energies (solid squares) and charge rms radii (open squares) of a number of nuclei obtained from SHF with Lc40, Lc92 and Lc134 from those measured in experiments. The bands indicate a deviation within  $\pm 2\%$ .

divided by the corresponding empirical Helm form factors. The proton and neutron form factors of other isotopes or elements can be obtained from a generalized Helm-like empirical parametrization given in the Appendix where the proton and neutron form factors are distinguished and parameterized as functions of the neutron skin thickness of  $^{208}\text{Pb}$  by fitting the results obtained from SHF calculations with Lc40, Lc92 and Lc134. In addition, also indicated in Fig. 3 is the momentum transfer  $q_m$  corresponding to a value of  $E_R = 100$  keV which represents the possible maximum cutoff among various experiments. However, we would like to emphasize that the upper limits of the recoil energy  $E_R$  usually vary significantly in different DM direct detection experiments, and here we just select a relatively large recoil energy of 100 keV as an example to see the possible symmetry energy effects on the proton and neutron form factors in different nuclei. In calculations of the scattering cross sections in Eq. (14) for each experiment, one must use the recoil energy region given by each experiment. It is seen from Fig. 3 that, for the nucleus  $^{28}\text{Si}$  with equal proton and neutron numbers, the symmetry energy effect is tiny and the SHF calculations with Lc40, Lc92 and Lc134 predict almost the same form factors for neutrons and protons, which are further in good agreement with the empirical Helm form factor for  $q \leq q_m$ . On the other hand, for the neutron-rich nucleus  $^{132}\text{Xe}$ , one can see a clear symmetry energy effect on the form factors, namely, a larger  $L(\rho_c)$  shifts the neutron form factor to lower  $q$  values while shifts slightly the proton form factor to higher  $q$  values with the empirical Helm form factor in between, leading to an isospin splitting between the proton and neutron form factors with respect to the  $q$  value. These features actually reflect the symmetry energy effects on the neutron skin thickness, namely, increasing the value of  $L(\rho_c)$  increases the rms radius of neutrons and reduces slightly the rms radius of protons, and thus leads to a larger neutron skin thickness as shown in Fig. 1.

Since the effective form factor (Eq. (12)) should be used to analyze the DM signals for general cases, it is expected that the isospin splitting between the proton and neutron form factors would cause significant effects on the effective form factor, especially for a negative  $g_{np}$  which could cause strongly destructive interference of DM scattering with protons and neutrons. On the other hand, the presence of different isotopes with comparable abundances in some detector target elements (e.g., xenon) suggests that it is better to study the averaged effective form factors defined as

$$|F^{\text{ave}}(E_R)|^2 = \frac{\sum_A \eta_A N_T^A A^2 |F_A(q(E_R))|^2}{\sum_A \eta_A N_T^A A^2}. \quad (22)$$

This is illustrated in Fig. 4 where the averaged effective form factor is plotted as a function of  $E_R$  for Si (left panels) and Xe (right panels) from SHF calculations with Lc40, Lc92 and Lc134. The results from the empirical Helm form factor with  $F_A^{\text{p,n}}(q) = F_A^{\text{Helm}}(q)$  are also included for comparison. In Fig. 4, two cases for the DM are considered: one is for the standard isospin-invariant DM with  $g_{np} = 1.0$  (upper panels) and the other is for the IVDM with  $g_{np} = -0.7$

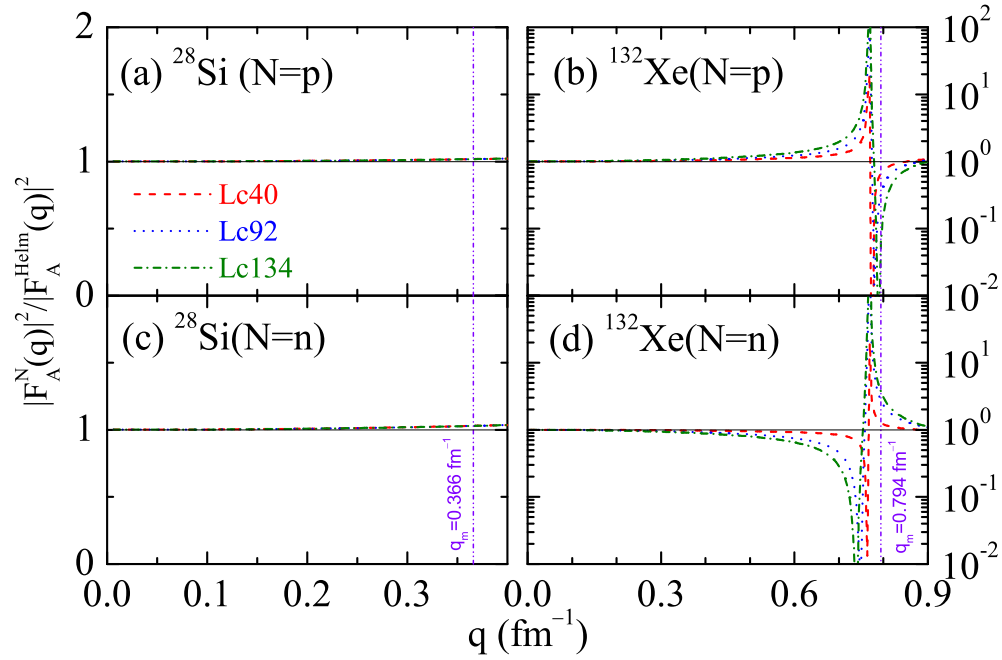


Figure 3: (Color online) Proton (upper panels) and neutron (lower panels) form factors divided by the corresponding empirical Helm form factors as functions of momentum transfer  $q$  for  $^{28}\text{Si}$  (left panels) and  $^{132}\text{Xe}$  (right panels) obtained from SHF with Lc40, Lc92 and Lc134. The momentum transfer  $q_m$ , corresponding to a value of  $E_R = 100$  keV, is indicated by dash-dot-dotted lines.

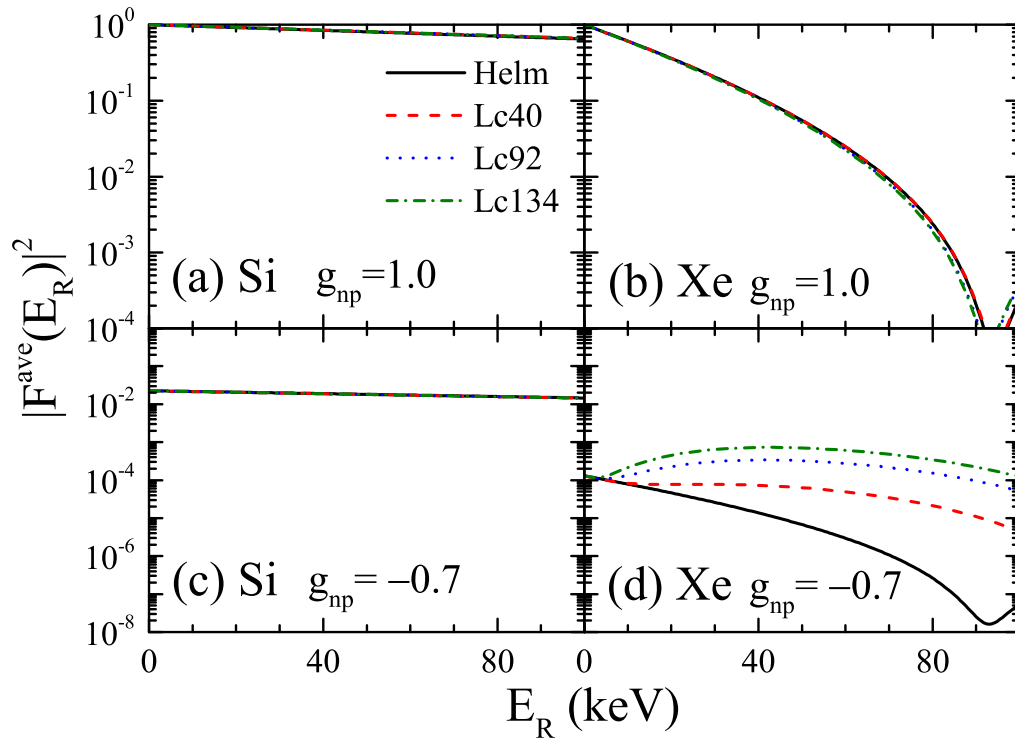


Figure 4: (Color online) The averaged effective form factor as a function of recoil energy  $E_R$  for Si (left panels) and Xe (right panels) with  $g_{np} = 1.0$  (upper panels) and  $g_{np} = -0.7$  (lower panels) obtained from SHF with Lc40, Lc92 and Lc134. The empirical Helm form factor is also included for comparison.



(lower panels). It should be pointed out that  $g_{\text{np}} = -0.7$ , firstly suggested by Feng *et al.* [22], leads to nearly complete destructive interference of the scattering amplitudes for DM-proton and DM-neutron collisions in Xe target and gives maximum suppression of the sensitivity for Xe-based detectors if the empirical Helm form factor is adopted. For such kind of IVDM, the confidence region of CDMS-II(Si) and the XENON100 exclusion contours are consistent with each other [34]. As will be shown later, for IVDM with  $g_{\text{np}} = -0.7$ , both the results from recent LUX [12] and the most recent SuperCDMS(Ge) [13] are also consistent with the confidence region of CDMS-II(Si). Theoretically, such negative values of  $g_{\text{np}}$  can arise, e.g., in models with a new light neutral gauge boson  $Z'$  [27, 31].

One can see from Fig. 4 that the negative  $g_{\text{np}}$  (i.e.,  $-0.7$ ) indeed causes strongly destructive interference of DM scattering with protons and neutrons for both Si and Xe targets and thus the averaged effective form factor with  $g_{\text{np}} = -0.7$  is strongly suppressed compared to its value with  $g_{\text{np}} = 1.0$ . Furthermore, it is interesting to see from Fig. 4 that for  $g_{\text{np}} = 1.0$ , the averaged effective form factors of both Si and Xe targets from SHF calculations with Lc40, Lc92 and Lc134 are in a very good agreement with the corresponding results from the empirical Helm form factors, indicating that there are essentially no symmetry energy effects. However, for  $g_{\text{np}} = -0.7$ , one can see that the averaged effective form factors of Xe target display very different behaviors for different distributions from SHF calculations with Lc40, Lc92 and Lc134 as well as that from the empirical charge distributions, although the averaged effective form factors of Si target are essentially the same for these different distributions. These features indicate that the symmetry energy effect is tiny for the averaged effective form factor of Si target but is very strong for that of Xe target in the case of  $g_{\text{np}} = -0.7$ . This is due to the fact that for a negative  $g_{\text{np}}$ , the scattering amplitudes for DM-proton and DM-neutron collisions may interfere destructively, and the DM particle is almost completely decoupled from the Xe isotopes, i.e.  $F(E_{\text{R}}) \approx 0$  (see panel (d) of Fig. 4), especially for  $g_{\text{np}} \approx -0.7$  [22]. In this case, a small difference between  $F_{\text{A}}^{\text{p}}$  and  $F_{\text{A}}^{\text{n}}$  may lead to a significant change for the effective form factor. As a result, the form factor of Xe exhibits a very strong symmetry energy effect for  $g_{\text{np}} = -0.7$ , namely, a larger  $L(\rho_{\text{c}})$  value leads to a larger form factor as shown in panel (d) of Fig. 4. In particular, one can see that the averaged effective form factors of Xe target from SHF calculations with Lc40, Lc92 and Lc134 can be significantly larger than that from the empirical Helm form factor in a large range of recoil energy. This implies that the symmetry energy with a larger  $L(\rho_{\text{c}})$  (and thus a larger neutron skin thickness) can give a more significant enhancement for the effective DM-nucleus form factors in Eq. (7) when the IVDM with  $g_{\text{np}} = -0.7$  is considered. Therefore, for  $g_{\text{np}} = -0.7$ , one can expect a significant enhancement for the sensitivity of the Xe-based detectors to the DM-proton cross sections by taking into account the form factor effects due to different symmetry energies compared with the corresponding result using the empirical Helm form factor in analyzing the experimental data.

## B. Form factor effects on the extraction of DM-proton cross sections

To see the effects of the form factor and the isospin-violation factor  $g_{\text{np}}$  on the extraction of elastic spin-independent DM-proton cross sections  $\sigma_{\text{p}}$  in DM direct detection experiments, we show in Fig. 5 the results of the 90% confidence level (C.L.) limits from XENON100 [11], LUX [12] and SuperCDMS(Ge) [13] along with the 90% C.L. favored regions from CDMS-II(Si) [8] in  $m_{\chi}$ - $\sigma_{\text{p}}$  plane for  $g_{\text{np}} = 1.0$  (left panel) and  $g_{\text{np}} = -0.7$  (right panel) with form factors from the empirical charge distributions and SHF calculations with MSL1 by varying  $L(\rho_{\text{c}})$  from 40.5 MeV to 134.2 MeV. For the results from SuperCDMS(Ge), only the mass region less than 30 GeV is shown since no data are available for  $m_{\chi} > 30$  GeV [13]. In these analyses, we use the standard astrophysical parameters in the Standard Halo Model, namely, a Maxwell-Boltzmann distribution for  $f(v)$  with  $v_0 = 220$  km/s and Galactic escape velocity  $v_{\text{esc}} = 544$  km/s, and a DM density of  $\rho_{\chi} = 0.3$  GeV/cm<sup>3</sup> [68, 69].

In Fig. 5, the form factor effects due to the symmetry energy and the effects from  $g_{\text{np}}$  are considered through dividing the experimental results by the degradation factor  $D_{\text{p}}$  as discussed earlier. In particular, for XENON100, we assume that the energy resolution is dominated by Poisson fluctuations in the number of photoelectrons (PE) as in Ref. [34]. We use S1 efficiency obtained from Fig. 1 of Ref. [11] and the scintillation efficiency  $\mathcal{L}_{\text{eff}}$  from Fig. 1 of Ref. [59], respectively, and integrate the differential rate over S1 from 3 to 30 PE to get the total rate. For the LUX analysis which is similar with XENON100's, the signal region is limited within 2 to 30 PE and the efficiencies are taken from Fig. 1 of Ref. [12]. For CDMS-II(Si), we use the acceptance from Fig. 1 of Ref. [9], and choose an energy interval between 7 keV and 100 keV in the analysis. For SuperCDMS(Ge), with the efficiency from Fig. 1 of Ref. [13], we use the signal region in the range 1.6 – 10 keV in the calculations as in Ref. [13]. Furthermore, since XENON100 reported 2 candidate events in the low recoil energy region, we calculate the degradation factor according to Eq. (21) instead of Eq. (14) to take into account the effects due to shape changing of the recoil spectrum as we will show later. Similarly, for LUX, we follow the analysis in Ref. [70] and calculate the degradation factor according to Eq. (21) by using one observed event (with S1 = 3.1 PE). For CDMS-II(Si) and SuperCDMS(Ge) that focus on the light DM, we have checked that the shape changing of their recoil spectra can be negligible and Eq. (14) is thus applied to evaluate the degradation factor.

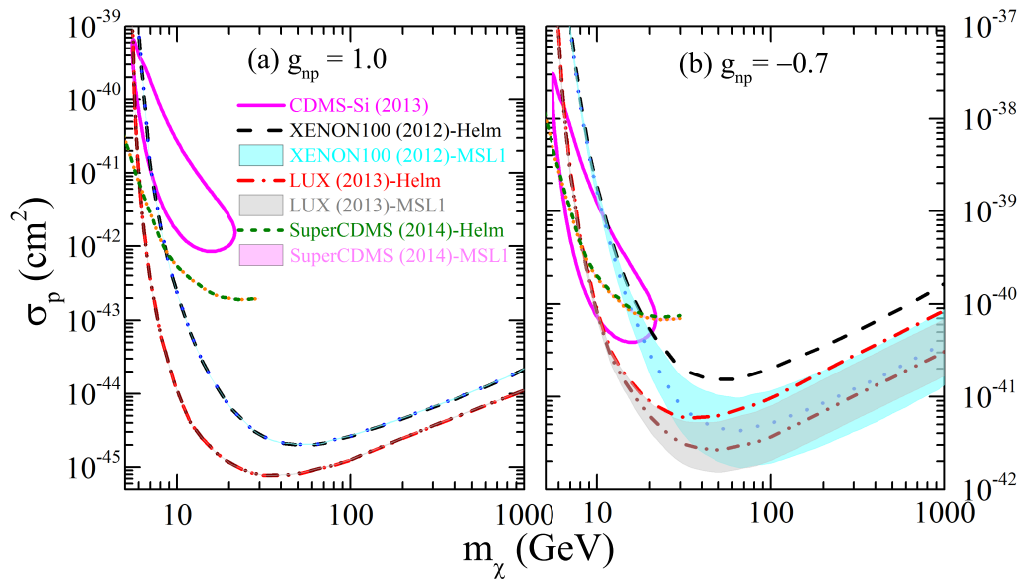


Figure 5: (Color online) Results of 90% confidence level (C.L.) limits from XENON100, LUX and SuperCDMS(Ge) together with 90% C.L. favored regions from CDMS-II(Si) in  $m_\chi$ - $\sigma_p$  plane for  $g_{np} = 1.0$  (left panel) and  $g_{np} = -0.7$  (right panel) with form factors from the empirical charge distributions (Helm) and SHF calculations with MSL1 by varying  $L(\rho_c)$  from 40.5 MeV to 134.2 MeV.

For the isospin-invariant DM with  $g_{np} = 1.0$ , one can see from Fig. 5 that the CDMS-II(Si) results are in some tension with the upper limit placed by the XENON100 experiment, and they become in even strong disagreement with the upper limits set by the recent LUX [12] experiment and the more recent SuperCDMS(Ge) [13] experiment. However, for the IVDM with  $g_{np} = -0.7$ , one can see that the tension between CDMS-II(Si) and XENON100 is essentially disappeared as found by Frandsen *et al.* [34]. Furthermore, it is remarkable to see from the right panel of Fig. 5 that the disagreement of the CDMS-II(Si) results with LUX and SuperCDMS(Ge) can also be largely ameliorated within the framework of IVDM with  $g_{np} = -0.7$  (We note that a similar conclusion is also obtained in Ref. [71]). Therefore, these results indicate that IVDM indeed provides a very promising mechanism to reconcile the tension among various experiments. It should be mentioned here that although  $g_{np} = -0.7$  leads to a maximum suppression for the sensitivity of Xe-based detector for the empirical Helm form factor, it does not for the more realistic SHF form factors as will be shown later.

Furthermore, it is interesting to see that, although there are essentially no form factor effects on the extracted spin-independent DM-proton cross sections  $\sigma_p$  in different experiments in the case of isospin-invariant DM with  $g_{np} = 1.0$ , the form factor effects can significantly affect the extraction of  $\sigma_p$  for the Xe-based experiments (XENON100 and LUX) in the case of IVDM with  $g_{np} = -0.7$ . Therefore, our results indicate that, for isospin-invariant DM, the widely used empirical Helm form factor is well grounded and this is consistent with our previous discussions about the form factor effects. On the other hand, for IVDM with  $g_{np} = -0.7$ , using the form factors obtained from SHF calculations in MSL1 with varied  $L(\rho_c)$  values generally increases the sensitivity of the Xe-based detectors (XENON100 and LUX) compared with using the empirical Helm form factor, and a larger  $L(\rho_c)$  value, which leads to a larger neutron skin thickness in Xe isotopes, generally leads to a stronger sensitivity of the Xe-based detectors. This form factor effect becomes more pronounced with the increment of the DM mass  $m_\chi$ . While the form factor effect is about 20% for the DM mass of  $m_\chi \approx 8$  GeV, it can become very significant for the DM with mass above a few tens GeV. For  $m_\chi = 20$  GeV, which roughly corresponds to the DM mass upper limit of CDMS-II(Si) bounds, the sensitivities of XENON100 and LUX can be enhanced by a factor of 3 using the form factor with  $L(\rho_c) = 134.2$  MeV compared with that using the empirical Helm form factor. In particular, the sensitivities can have a factor of more than 10 improvement for  $m_\chi \geq 80$  GeV where many constraints for supersymmetric WIMPs have been put by the data from LHC [72]. On the other hand, the relative variation between the results extracted from the Helm form factor and the SHF calculations is small ( $< 7\%$ ) for SuperCDMS(Ge) and it can be negligible ( $< 0.5\%$ ) for CDMS-II(Si) for which the results from the SHF calculations are not shown in Fig. 5.

The DM mass dependence of the form factor effects observed in XENON100 and LUX for  $g_{np} = -0.7$  can be understood as a result of the shape changing of the expected recoil spectra for varied  $m_\chi$  due to the enhancement effects of the form factors when we take the symmetry energy effects into account as discussed in the previous subsection. Shown in Fig. 6 is the normalized DM-xenon recoil spectrum  $f_s(E_R)$  for  $m_\chi = 8$  GeV, 20 GeV and

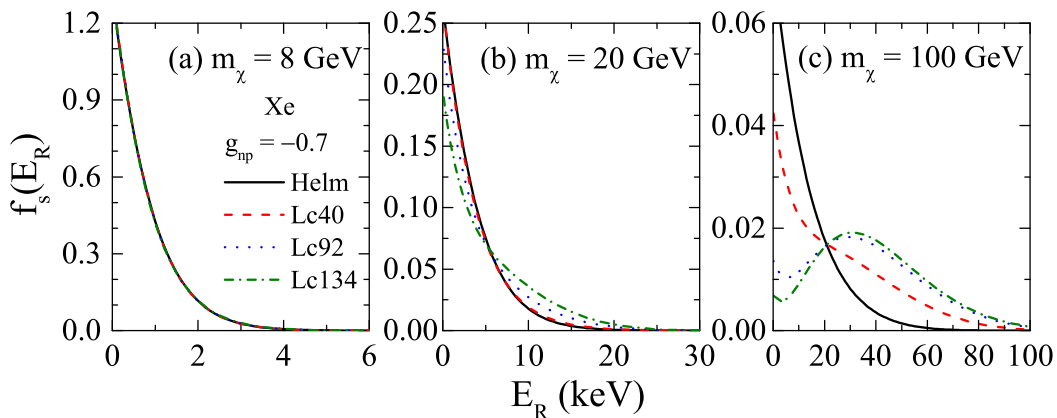


Figure 6: (Color online) The normalized DM-xenon recoil spectrum  $f_s(E_R)$  with  $g_{np} = -0.7$  for  $m_\chi = 8$  GeV (panel (a)),  $m_\chi = 20$  GeV (panel (b)) and  $m_\chi = 100$  GeV (panel (c)), respectively. Cases for different form factors from the empirical Helm charge distribution (black solid lines) and SHF calculations with MSL1 by varying  $L(\rho_c)$  from 40.5 MeV to 134.2 MeV are shown in the figure. For comparison, spectra calculated with Helm form factors for isospin-invariant cases ( $g_{np} = 1$ ) are also shown.

100 GeV with  $g_{np} = -0.7$  and various form factors from SHF calculations with Lc40, Lc92 and Lc134 as well as the empirical Helm form factor. We note that for  $g_{np} = 1.0$ , the  $f_s(E_R)$  essentially does not depend on the variation of the form factors and the results are almost the same as that from the empirical Helm form factor with  $g_{np} = -0.7$ . It is very interesting to see from Fig. 6 that for the case with  $g_{np} = -0.7$ , although the form factor effect essentially does not change or only slightly modifies the predicted normalized DM-xenon recoil spectra for light DM (see, e.g., Figs. 6 (a) and (b)), it can drastically change the shape of the recoil spectra for heavy DM (see, e.g., Fig. 6 (c)). For both XENON100 and LUX, we have considered this spectrum shape changing effect in Eq. (21) by multiplying Eq. (14) by another term  $R_{\text{ex}}(\sigma_N^{\text{up}})/R_{\text{ex}}(\sigma_p^{\text{up}})$  for the degradation factor, which will result in, e.g.,  $\sim 14\%$  ( $\sim 7\%$ ) enhancement of the upper limit of  $\sigma_p$  from XENON100 (LUX) relative to the results obtained from Eq. (14) for the Lc134 case with  $m_\chi = 100$  GeV. More specifically, one can see from Fig. 6 that for heavier DM, the expected DM-xenon recoil spectra become harder and thus the effective form factors are typically probed at higher momentum transfer, and this will significantly enhance the effects caused by different form factors (see, e.g., Fig. 4 (d)) adopted for the  $E_R$  integration in the numerator of r.h.s of Eq. (14), leading to the observed DM mass dependence of the form factor effects in XENON100 and LUX for  $g_{np} = -0.7$ .

It is also very interesting to see that for the case with  $g_{np} = -0.7$ , the bounds of XENON100 and LUX overlap with each other in the mass region of  $m_\chi \geq 70$  GeV although the LUX gives much more stringent limit on the spin-independent elastic DM-proton scattering cross section than XENON100 in the lower mass region as shown in the right panel of Fig. 5. This can also be explained as a result of the shape changing of the expected recoil spectrum for varied  $m_\chi$  as shown in Fig. 6. Particularly, Fig. 6 suggests that a significant fraction of the events is expected at larger recoil energies for heavier DM, and this is especially the case for the IVDM with  $g_{np} = -0.7$  and SHF form factors with Lc92 and Lc134 where one can see the non-standard recoil spectra peaked around  $E_R = 30$  keV. Since LUX adopts a relatively small energy range, i.e. 3.0 – 22.1 keV [12], compared with XENON100 where 6.6 – 43.3 keV is adopted [11], it thus exhibits relatively weaker sensitivity than XENON100 for heavier DM. As a matter of fact, even for the isospin-invariant case where the form factor effects are negligible as shown in Fig. 5 (a), the sensitivity of LUX becomes relatively weaker with the increment of  $m_\chi$  compared with that of XENON100. It should be mentioned that the small form factor effect observed for SuperCDMS(Ge) in Fig. 5 (b) is also partially due to the smaller threshold energy cut, i.e., 1.6 – 10.0 keV [13]. Our results imply that the non-standard recoil spectra shown in Fig. 6 (c) may provide an extremely important experimental evidence for non-standard dark matter interactions and they also give valuable information on the direct detection of IVDM.

### C. Form factor effects with various isospin-violation factor $g_{np}$

In above calculations for the case of IVDM, we have fixed the isospin-violation factor at  $g_{np} = -0.7$ . As mentioned earlier, for the specific IVDM with  $g_{np} = -0.7$ , the sensitivity of Xe-based detectors is maximumly suppressed when the empirical Helm form factor is used and the tension among various experiments using different target elements has been shown to be largely ameliorated. For more realistic SHF form factors, it is interesting to see how the form factor

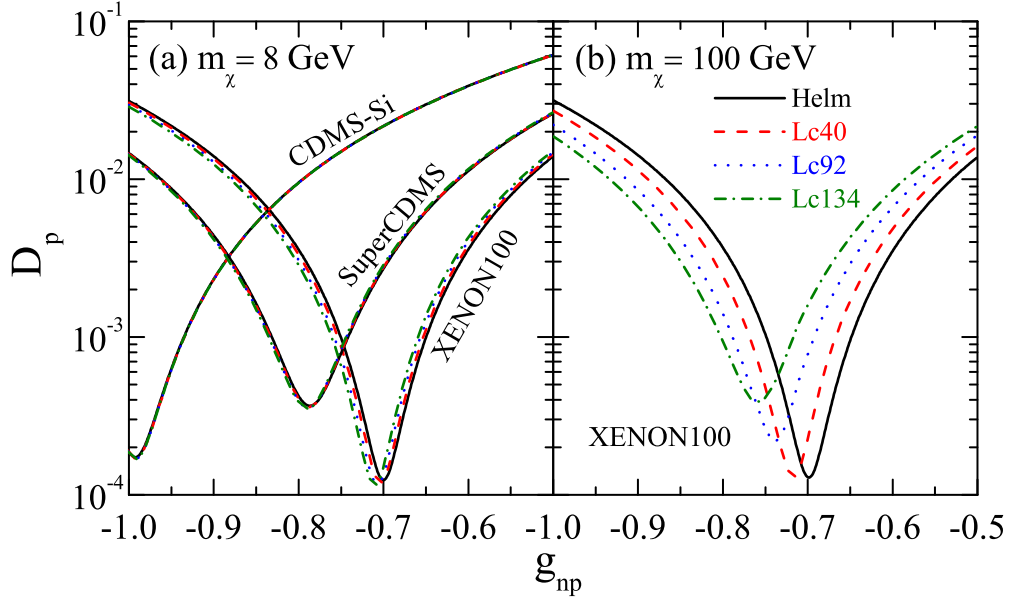


Figure 7: (Color online) Degradation factor  $D_p$  as a function of the isospin-violation factor  $g_{np}$  obtained by using the empirical Helm form factors as well as the form factors from SHF calculations with Lc40, Lc92 and Lc134 for  $m_\chi = 8$  GeV (panel (a)) and  $m_\chi = 100$  GeV (panel (b)). For  $m_\chi = 8$  GeV, the results of CDMS-II(Si), SuperCDMS(Ge) and XENON100 are shown while only the results of XENON100 are shown for  $m_\chi = 100$  GeV.

effects change with more general values of the isospin-violation factor  $g_{np}$ . Following the method by Feng *et al.* [23], we study in the following how the form factor effects change for various isospin-violation factor  $g_{np}$ . Shown in Fig. 7 is the degradation factor  $D_p$  as a function of the isospin-violation factor  $g_{np}$  obtained by using the empirical Helm form factors as well as the form factors from SHF calculations with Lc40, Lc92 and Lc134 for  $m_\chi = 8$  GeV (panel (a)) and  $m_\chi = 100$  GeV (panel (b)). Since both XENON100 and LUX are Xe-based experiments and their results have similar dependence on the  $g_{np}$  and the symmetry energy, we thus only consider CDMS-II(Si), SuperCDMS(Ge) and XENON100 in Fig. 7 (a) for  $m_\chi = 8$  GeV. In addition, for  $m_\chi = 100$  GeV, the form factor effect is negligible for CDMS-II(Si) and relatively small for SuperCDMS(Ge) which adopts a small threshold energy cut and has been designed especially for light DM searching, we thus only show the results of XENON100 (panel (b)).

It is seen from Fig. 7 that generally the sensitivity of each detector is significantly suppressed for a negative  $g_{np}$  within the range of  $-1.0 < g_{np} < -0.5$  due to destructive interference between DM-neutron and DM-proton scattering amplitudes as pointed out in Ref. [22, 23]. However, the  $D_p$  reaches its minimum value (where the detector is most insensitive) at different values of  $g_{np}$  for different detectors due to the different compositions and distributions of neutrons and protons in each target element of the detector. In particular, one can see that the corresponding value of  $g_{np}$  which leads to a minimum value of  $D_p$ , denoted as  $g_{np}^{\min}$ , is about  $-0.993$ ,  $-0.787$  and  $-0.700$  for CDMS-II(Si), SuperCDMS(Ge) and XENON100, respectively, for the case of  $m_\chi = 8$  GeV when the empirical Helm form factor is used. For  $m_\chi = 8$  GeV, the form factor effect is very small for CDMS-II(Si) and the largest relative variation with respect to the results from the empirical Helm form factor when  $L(\rho_c)$  varies from 40.2 MeV to 134.2 MeV is 1.26% at  $g_{np} = -0.997$ . The largest relative variation due to the form factor effect is 6.22% at  $g_{np} = -0.818$  for SuperCDMS(Ge), and it becomes 47.11% at  $g_{np} = -0.686$  for XENON100. As a matter of fact, a clear shift of curves for the Xe-based detectors calculated with different form factors has been already seen even for such a small DM mass in Fig. 7 (a). These features indicate that the form factor effect can be already pronounced for XENON100 even for a small mass DM with  $m_\chi = 8$  GeV. For XENON100, one can see from Fig. 7(b) that the form factor effect becomes very strong for  $m_\chi = 100$  GeV. In particular, a larger  $L(\rho_c)$  value gives significantly stronger sensitivity of the detectors and the largest relative variation due to the form factor effect is 952.30% (almost one order) at  $g_{np} = -0.695$ .

Furthermore, one can see from Fig. 7 that the value of  $g_{np}^{\min}$  also depends significantly on the form factor, and it is  $-0.716$ ,  $-0.737$  and  $-0.754$  for the SHF form factor with  $L(\rho_c) = 40.2$ , 92.4 and 134.2 MeV, respectively, smaller than  $g_{np} = -0.7$  for the empirical Helm form factor. In addition, it is very interesting to see that, while using the SHF form factors enhances the sensitivity of the Xe-based detector relative to the case with Helm form factor for  $g_{np} \geq -0.7$ , it suppresses the sensitivity for  $g_{np} < -0.7$ . These features indicate that the form factor effects can either enhance or suppress the sensitivity of the detector relative to the Helm's case depending on the specific value adopted for  $g_{np}$ . It is also very interesting to see that one cannot find a  $g_{np}$  value such that  $D_p \rightarrow 0$ , leading to zero



sensitivity for scattering off the elements, and this is mainly due to the fact that the elements have multiple isotopes and completely destructive interference cannot be simultaneously achieved for all isotopes [22, 23]. We would like to point out that even for elements with only one naturally abundant isotope, one still cannot find a  $g_{np}$  value such that  $D_p \rightarrow 0$  since the neutron form factor is generally different from the proton form factor in a nucleus.

The above results indicate that, the form factor effect can not only significantly change the sensitivities of the detectors, but also affect the interaction behaviors of the target element with the isospin-violating DM in various isospin-violating regions we are interested in for DM direct detection experiments. In future when different direct detection experiments using various target elements had specify the DM signals precisely, one may determine simultaneously the isospin-violation factor  $g_{np}$  and the form factor (and thus the neutron skin thickness as well as the symmetry energy), especially if the IVDM particle has a larger mass of above tens of GeV. Conversely, our results indicate that precise knowledge on the symmetry energy or the neutron skin thickness (and thus the neutron and proton form factors) of  $^{208}\text{Pb}$  is of critical importance for the direct detection of IVDM using Xe-based detectors. In particular, the future experiment PREX-II [73] at JLab is expected to improve significantly the measurement accuracy of the neutron skin thickness for  $^{208}\text{Pb}$  and thus could make important contribution to this issue.

#### IV. CONCLUSION

In the present work, we have shown that isospin-violating dark matter (IVDM) indeed provides a possible mechanism to ameliorate the tension among recent direct detection experiments, including CDMS-II(Si), XENON100, LUX, and SuperCDMS(Ge). For IVDM, we have demonstrated that the results of the DM direct detection experiments based on neutron-rich target nuclei, e.g., Xe-based detector, may strongly depend on the density slope  $L(\rho_c)$  of the symmetry energy at a subsaturation cross density  $\rho_c \approx 0.11\text{fm}^{-3}$ , which is presently largely unknown and uniquely determines the neutron skin thickness and thus the relative difference of neutron and proton form factors of the target nuclei.

In particular, using the proton and neutron form factors obtained from Skyrme-Hartree-Fock calculations by varying the  $L(\rho_c)$  within the uncertainty region set by the latest model-independent measurement of the neutron skin thickness from PREX experiment at JLab, we have found that although the form factor effects on the extracted bounds on DM-proton cross sections are negligible in the direct detection for isospin-invariant DM, they could become critically important in the detection for IVDM. Especially, for IVDM with neutron-to-proton coupling ratio fixed to  $f_n/f_p = -0.7$  in the mass region constrained by CMDS-II(Si), the form factor effect may enhance the sensitivity of Xe-based detectors (e.g., XENON100 and LUX) to the DM-proton cross section by a factor of 3, compared with the results using the empirical Helm nuclear form factors extracted from charge distributions. This form factor effect can even enhance the sensitivity by more than a factor of 10 for such kind of IVDM with mass larger than 80 GeV.

Furthermore, we have found that the form factor effect can significantly modify the recoil spectrum of Xe-based detectors for heavy IVDM with  $f_n/f_p = -0.7$ . We have also studied how the form factor effects change with the variation of  $f_n/f_p$  and found that the  $f_n/f_p$  value maximumly suppressing the sensitivity of the detector may depend on the form factor, and the form factor effects can either enhance or suppress the sensitivity of the detector relative to the Helm's case depending on the specific value adopted for  $f_n/f_p$ . Our results imply that the precise determination of the symmetry energy or the neutron skin thickness (and thus the neutron and proton form factors) of  $^{208}\text{Pb}$  is extremely useful for the direct detection of IVDM based on detectors with neutron-rich targets (e.g., xenon).

#### Acknowledgments

The authors would like to thank Fei Gao for useful discussions. This work was supported in part by the NNSF of China under Grant Nos. 11275125 and 11135011, the Shanghai Rising-Star Program under grant No. 11QH1401100, the ‘‘Shu Guang’’ project supported by Shanghai Municipal Education Commission and Shanghai Education Development Foundation, the Program for Professor of Special Appointment (Eastern Scholar) at Shanghai Institutions of Higher Learning, and the Science and Technology Commission of Shanghai Municipality (11DZ2260700).

#### Appendix: An empirical parametrization for proton and neutron form factors

Shown in Fig. 3 are the proton and neutron form factors as functions of momentum transfer for  $^{28}\text{Si}$  and  $^{132}\text{Xe}$  from SHF calculations with Lc40, Lc92 and Lc134. The results for other isotopes of Si and Xe as well as Ge isotopes can also be calculated in the same approach. Thanks to the approximately linear relationship between the symmetry energy density slope parameter  $L(\rho_c)$  and the neutron skin thickness  $\Delta r_{np}$  of  $^{208}\text{Pb}$ , it is possible to approximate the proton and neutron form factors obtained from SHF calculations with varied  $L(\rho_c)$  by analytical parameterizations

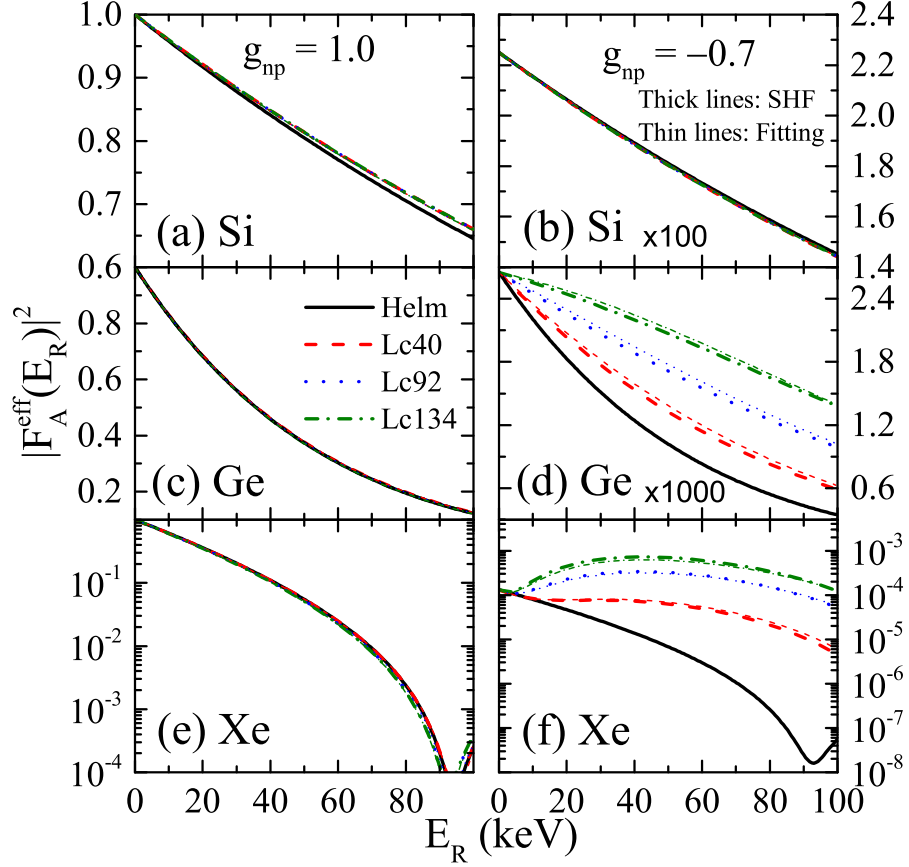


Figure 8: (Color online) The averaged effective form factors as functions of recoil energy  $E_R$  for Si (upper panels), Ge (middle panels) and Xe (lower panels) with  $g_{np} = 1.0$  (left panels) and  $g_{np} = -0.7$  (right panels) obtained from SHF with Lc40, Lc92 and Lc134 (thick lines) and from the empirical parametrization for proton and neutron form factors in Eq. (A.1) (thin lines) with  $\Delta r_{np} = 0.15$  fm,  $0.33$  fm and  $0.49$  fm. The empirical Helm form factor is also included for comparison.

with explicit dependence on the  $\Delta r_{np}$  of  $^{208}\text{Pb}$ . In particular, here we construct the analytical expressions for the proton and neutron form factors separately according to Helm-like form factor with an additional term to consider isospin dependence and the symmetry energy effects (and thus  $\Delta r_{np}$  of  $^{208}\text{Pb}$ ), i.e.,

$$F_A^{n(p)}(q) = 3 \frac{j_1(qr_{p(n)})}{qr_{p(n)}} \times e^{-(qs)^2/2}, \quad (\text{A.1})$$

where the effective proton (neutron) distribution radius is parameterized as

$$r_{p(n)}^2 = c_{p(n)}^2 + \frac{7}{3}\pi^2 a^2 - 5s^2, \quad (\text{A.2})$$

with

$$c_p = r_0 A^{\frac{1}{3}} + e - d \cdot (\Delta r_{np})^{\frac{1}{4}} \frac{Z(N-Z)}{A^2}, \quad (\text{A.3})$$

$$c_n = r_0 A^{\frac{1}{3}} + e + d \cdot \Delta r_{np} \frac{N(N-Z)}{A^2}. \quad (\text{A.4})$$

Compared with the parametrization of Helm form factor (i.e., Eq. (16)), the parametrization here includes an additional term, namely, the last term in Eq. (A.3) and Eq. (A.4). In addition, our parametrization here distinguishes protons and neutrons, and depends on explicitly the proton and neutron numbers of the nucleus and the  $\Delta r_{np}$  of  $^{208}\text{Pb}$ .

By fitting a number of proton and neutron form factors calculated from SHF approach with varied symmetry energies, including the 9 stable Xe isotopes, 5 stable Ge isotopes and 3 stable Si isotopes with the symmetry energy



Table I: Parameters in the empirical parametrization of Eq. (A.1) for proton and neutron form factors.

	Proton	Neutron
$r_0$ (fm)	1.2249	1.1425
$d$ (fm)	5.6794	5.4433
$e$ (fm)	-0.0436	0.2737
$a$ (fm)	0.2898	0.2200
$s$ (fm)	0.8521	0.9752

density slope parameter  $L(\rho_c)$  varying from 40.5 MeV to 134.2 MeV, we obtain all parameters in the above expressions and they are listed in Table I. In order to test the quality of the above parametrization, we compare in Fig. 8 the averaged effective form factors as functions of  $E_R$  for Si, Ge and Xe using the above parameterized proton and neutron form factors with the results obtained from the SHF approach. It is very interesting to see that one can indeed simply use just one set of parameters given in Table I to well describe the proton and neutron form factors in different nuclei in a large mass region with very different values of the symmetry energy density slope parameter  $L(\rho_c)$  (i.e.,  $\Delta r_{np}$  of  $^{208}\text{Pb}$ ).

- 
- [1] **Planck** Collaboration, P. A. R. Ade et al., *Planck 2013 results. XVI. Cosmological parameters*, arXiv:1303.5076.
- [2] G. Steigman and M. S. Turner, *Cosmological Constraints on the Properties of Weakly Interacting Massive Particles*, *Nucl. Phys. B* **253** (1985) 375.
- [3] G. Jungman, M. Kamionkowski, and K. Griest, *Supersymmetric dark matter*, *Phys. Rept.* **267** (1996) 195 [hep-ph/9506380].
- [4] M. W. Goodman and E. Witten, *Detectability of Certain Dark Matter Candidates*, *Phys. Rev. D* **31** (1985) 3059.
- [5] **CoGeNT** Collaboration, C. E. Aalseth et al., *Results from a Search for Light-Mass Dark Matter with a P-type Point Contact Germanium Detector*, *Phys. Rev. Lett.* **106** (2011) 131301 [arXiv:1002.4703].
- [6] C. Savage et al., *Compatibility of DAMA/LIBRA dark matter detection with other searches*, *JCAP* **0904** (2009) 010 [arXiv:0808.3607].
- [7] **CRESST II** Collaboration, G. Angloher et al., *Results from 730 kg days of the CRESST-II Dark Matter Search*, *European Physical Journal C* **72** (2012) 1971 [arXiv:1109.0702].
- [8] **CDMS II** Collaboration, R. Agnese et al., *Silicon Detector Results from the First Five-Tower Run of CDMS II*, *Phys. Rev. D* **88** (2013) 031104 [arXiv:1304.3706].
- [9] **CDMS II** Collaboration, R. Agnese et al., *Dark Matter Search Results Using the Silicon Detectors of CDMS II*, *Phys. Rev. Lett.* **111** (2013) 251301 [arXiv:1304.4279].
- [10] **XENON100** Collaboration, E. Aprile et al., *Dark Matter Results from 100 Live Days of XENON100 Data*, *Phys. Rev. Lett.* **107** (2011) 131302 [arXiv:1104.2549].
- [11] **XENON100** Collaboration, E. Aprile et al., *Dark Matter Results from 225 Live Days of XENON100 Data*, *Phys. Rev. Lett.* **109** (2012) 181301 [arXiv:1207.5988].
- [12] **LUX** Collaboration, D.S. Akerib et al., *First results from the LUX dark matter experiment at the Sanford Underground Research Facility*, *Phys. Rev. Lett.* **112** (2014) 091303 [arXiv:1310.8214].
- [13] **SuperCDMS** Collaboration, R. Agnese et al., *Search for Low-Mass WIMPs with SuperCDMS*, arXiv:1402.7137.
- [14] C. Savage, G. Gelmini, P. Gondolo, and K. Freese, *XENON10/100 dark matter constraints in comparison with CoGeNT and DAMA: Examining the  $L_{eff}$  dependence*, *Phys. Rev. D* **83** (2011) 055002 [arXiv:1006.0972].
- [15] D. Smith and N. Weiner, *Inelastic dark matter*, *Phys. Rev. D* **64** (2001) 043502 [arXiv:hep-ph/0101138].
- [16] M. T. Frandsen, F. Kahlhoefer, C. McCabe, S. Sarkar, and K. Schmidt-Hoberg, *Resolving astrophysical uncertainties in dark matter direct detection*, *JCAP* **024** (2012) 1201 [arXiv:1111.0292].
- [17] Y.-Y. Mao, L. E. Strigari, and R. H. Wechsler, *Connecting Direct Dark Matter Detection Experiments to Cosmologically Motivated Halo Models*, *Phys. Rev. D* **89** (2014) 063513 [arXiv:1304.6401].
- [18] R. C. Cotta, A. Rajaraman, T. M. P. Tait, and A. M. Wijangco, *Particle Physics Implications and Constraints on Dark Matter Interpretations of the CDMS Signal*, arXiv:1305.6609.
- [19] A. Kurylov and M. Kamionkowski, *Generalized analysis of weakly interacting massive particle searches*, *Phys. Rev. D* **69** (2004) 063503 [hep-ph/0307185].
- [20] F. Giuliani, *Are direct search experiments sensitive to all spin-independent WIMP candidates?*, *Phys. Rev. Lett.* **95** (2005) 101301 [hep-ph/0504157].
- [21] S. Chang, J. Liu, A. Pierce, N. Weiner and I. Yavin, *CoGeNT Interpretations*, *JCAP* **08** (2010) 018 [arXiv:1004.0697].
- [22] J. L. Feng, J. Kumar, D. Marfatia, D. Sanford, *Isospin-Violating Dark Matter*, *Phys. Lett. B* **703** (2011) 124-127 [arXiv:1102.4331].
- [23] J. L. Feng, J. Kumar, and D. Sanford, *Xenophobic Dark Matter*, *Phys. Rev. D* **88** (2013) 015021 [arXiv:1306.2315].
- [24] J. L. Feng, J. Kumar, D. Marfatia, and D. Sanford, *Isospin-Violating Dark Matter Benchmarks for Snowmass 2013*,

arXiv:1307.1758.

- [25] K. I. Nagao and T. Naka, *Isospin-violating dark matter search by nuclear emulsion detector*, *Prog. Theor. Exp. Phys.* **B 02** (2013) 043 [arXiv:1205.0198].
- [26] V. Cirigliano, M. L. Graesser, G. Ovanessian, and I. M. Shoemaker, *Shining LUX on Isospin-Violating Dark Matter Beyond Leading Order*, arXiv:1311.5886.
- [27] M. T. Frandsen, F. Kahlhoefer, S. Sarkar, and K. Schmidt-Hoberg, *Direct detection of dark matter in models with a light Z*, *JHEP* **1109** (2011) 128 [arXiv:1107.2118].
- [28] J. M. Cline and A. R. Frey, *Minimal hidden sector models for CoGeNT/DAMA events*, *Phys. Rev. D* **84** (2011) 075003 [arXiv:1108.1391].
- [29] E. Del Nobile, C. Kouvaris, F. Sannino, and J. Virkajarvi, *Dark Matter Interference*, *Mod. Phys. Lett. A* **27** (2012) 1250108 [arXiv:1111.1902].
- [30] X.-G. He, B. Ren, and J. Tandean, *Hints of standard model Higgs boson at the LHC and light dark matter searches*, *Phys. Rev. D* **85** (2012) 093019 [arXiv:1112.6364].
- [31] X. Gao, Z. Kang, and T. Li, *Origins of the isospin violation of dark matter interactions*, *JCAP* **01** (2013) 021 [arXiv:1107.3529].
- [32] N. Okada and O. Seto, *Isospin violating dark matter being asymmetric*, *Phys. Rev. D* **88** (2013) 063506 [arXiv:1304.6791].
- [33] J. D. Lewin and P. F. Smith, *Review of mathematics, numerical factors, and corrections for dark matter experiments based on elastic nuclear recoil*, *Astroparticle Phys.* **6** (1996) 87.
- [34] M. T. Frandsen et al., *The unbearable lightness of being: CDMS versus XENON*, *JCAP* **07** (2013) 023 [arXiv:1304.6066].
- [35] R. Helm, *Inelastic and Elastic Scattering of 187-Mev Electrons from Selected Even-Even Nuclei*, *Phys. Rev.* **104** (1956) 1466.
- [36] G. Duda, A. Kemper, and P. Gondolo, *Model Independent Form Factors for Spin Independent Neutralino-Nucleon Scattering from Elastic Electron Scattering Data*, *JCAP* **0704** (2007) 012 [hep-ph/0608035].
- [37] Y.Z. Chen, Y.Z. Luo, L. Li, H. Shen, and X.Q. Li, *Determining Nuclear Form factor for Detection of Dark Matter in Relativistic Mean Field Theory*, *Commun. Ther. Phys.* **55** (2011) 1059 [arXiv:1101.3049].
- [38] G. Go', V. De Donno, M. Anguiano and A.M. Lallena, *Nuclear proton and neutron distributions in the detection of weak interacting massive particles*, *JCAP* **11** (2012) 010 [arXiv:1211.1787].
- [39] R. Hofstadter, *Electron scattering and nuclear structure*, *Rev. Mod. Phys.* **28** (1956) 214.
- [40] B. Frois et al., *High Momentum Transfer electron Scattering from Pb-208*, *Phys. Rev. Lett.* **38** (1977) 152.
- [41] C. W. de Jager and C. de Vries, *Nuclear charge-density-distributions parameters*, *At. Data Nucl. Data Tables* **36** (1987) 495.
- [42] **PREX** Collaboration, S. Abrahamyan et al., *Measurement of the Neutron Radius of 208Pb Through Parity-Violation in Electron Scattering*, *Phys. Rev. Lett.* **108** (2012) 112502 [arXiv:1201.2568].
- [43] A. Ong, J. C. Berengut, and V. V. Flambaum, *The Effect of spin-orbit nuclear charge density corrections due to the anomalous magnetic moment on halonuclei*, *Phys. Rev. C* **82** (2010) 014320 [arXiv:1006.5508].
- [44] C.J. Horowitz et al., *Neutron star structure and the neutron radius of Pb-208*, *Phys. Rev. Lett* **86** (2001) 5647 [astro-ph/0010227].
- [45] B.A. Brown, *Neutron radii in nuclei and the neutron equation of state*, *Phys. Rev. Lett.* **85** (2000) 5296; S. Typel and B.A. Brown, *Neutron radii and the neutron equation of state in relativistic models*, *Phys. Rev. C* **64** (2001) 027302.
- [46] B.A. Li, L.W. Chen, and C.M. Ko, *Recent Progress and New Challenges in Isospin Physics with Heavy-Ion Reactions*, *Phys. Rep.* **464** (2008) 113 [arXiv:0804.3580].
- [47] Z. Zhang and L.W. Chen, *Constraining the symmetry energy at subsaturation densities using isotope binding energy difference and neutron skin thickness*, *Phys. Lett. B* **726** (2012) 234 [arXiv:1302.5327].
- [48] Topical Issue *Nuclear Symmetry Energy* edited by Bao-An Li, Angels Ramos, Giuseppe Verde, Isaac Vidana, *Eur. Phys. J. A* **50** (2014).
- [49] E. Chabanat, P. Bonche, P. Haensel, J. Meyer, and R. Schaeffer, *A Skyrme parametrization from subnuclear to neutron star densities*, *Nucl. Phys. A* **627** (1997) 710.
- [50] J. Friedrich and P.-G. Reinhard, *Skyrme-force parametrization: Least-squares fit to nuclear ground-state properties*, *Phys. Rev. C* **33** (1986) 335.
- [51] P. Klüpfel, P.-G. Reinhard, T.J. Bürvenich, and J.A. Maruhn, *Variations on a theme by Skyrme: A systematic study of adjustments of model parameters*, *Phys. Rev. C* **79** (2009) 034310 [arXiv:0804.3385].
- [52] L.W. Chen, C.M. Ko, B.A. Li, and J. Xu, *Density slope of the nuclear symmetry energy from the neutron skin thickness of heavy nuclei*, *Phys. Rev. C* **82** (2010) 024321 [arXiv:1004.4672].
- [53] L.W. Chen and J.Z. Gu, *Correlations between the nuclear breathing mode energy and properties of asymmetric nuclear matter*, *J. Phys. G* **39** (2012) 035104 [arXiv:1104.5407].
- [54] L.W. Chen, *Higher order bulk characteristic parameters of asymmetric nuclear matter*, *Sci. China: Phys. Mech. Astro.* **54** (Suppl. 1) (2011) s124 [arXiv:1101.2384].
- [55] L.W. Chen, *Nuclear matter symmetry energy and the symmetry energy coefficient in the mass formula*, *Phys. Rev. C* **83** (2011) 044308 [arXiv:1101.5217].
- [56] G. Gelmini and P. Gondolo, *WIMP annual modulation with opposite phase in Late-Infall halo models*, *Phys. Rev. D* **64** (2001) 023504 [hep-ph/0012315].
- [57] R. Schoenrich, J. Binney, and W. Dehnen, *Local Kinematics and the Local Standard of Rest*, *Mon. Not. R. Astron. Soc.* **403** (2010) 1829.
- [58] P. Ring and P. Schuck, *The nuclear many-body problem*, Springer, Berlin, 1980.

- [59] **XENON100** Collaborartion, E. Aprile et al., *Likelihood approach to the first dark matter results from XENON100*, *Phys. Rev. D* **84** (2011) 052003.
- [60] S. Yellin, *Finding an upper limit in the presence of an unknown background*, *Phys. Rev. D* **66** (2002) 032005.
- [61] R. Chen, B.J. Cai, L.W. Chen, B.A. Li, C. Xu, and J. Xu, *Single-nucleon potential decomposition of the nuclear symmetry energy*, *Phys. Rev. C* **85** (2012) 024305 [arXiv:1112.2936].
- [62] L.W. Chen, C.M. Ko, and B.A. Li, *Isospin-dependent properties of asymmetric nuclear matter in relativistic mean field models*, *Phys. Rev. C* **76** (2007) 054316 [arXiv:0709.0900].
- [63] F.J. Fattoyev, C.J. Horowitz, J. Piekarewicz, and G. Shen, *Relativistic effective interaction for nuclei, giant resonances, and neutron stars*, *Phys. Rev. C* **82** (2010) 055803 [arXiv:1008.3030].
- [64] F.J. Fattoyev and J. Piekarewicz, *Has a Thick Neutron Skin in Pb208 Been Ruled Out?*, *Phys. Rev. Lett.* **111** (2013) 162501 [arXiv:1306.6034].
- [65] M. Wang, G. Audi, A. H. Wapstra, F. G. Kondev, M. MacCormick, X. Xu, and B. Pfeiffer, *The Ame2012 atomic mass evaluation (II). Tables, graphs and references*, *Chin. Phys. C* **36** (2012) 1287.
- [66] I. Angeli, *A consistent set of nuclear rms charge radii: properties of the radius surface  $R(N,Z)$* , *At. Data Nucl. Data Tab.* **87** (2004) 185.
- [67] F. Le Blanc, L. Cabaret, E. Cottureau, J.E. Crawford, S. Essabaa, J. Genevey, R. Horn, G. Huber, J. Lassen, J.K.P. Lee, G. Le Scornet, J. Lettry, J. Obert, J. Oms, A. Ouchrif, J. Pinard, H. Ravn, B. Roussiere, J. Sauvage, and D. Verney, *Charge-radius change and nuclear moments in the heavy tin isotopes from laser spectroscopy: Charge radius of  $^{132}\text{Sn}$* , *Phys. Rev. C* **72** (2005) 034305.
- [68] M. C. Smith et al., *The RAVE Survey: Constraining the Local Galactic Escape Speed*, *Mon. Not. R. Astron. Soc.* **379** (2007) 755 [astro-ph/0611671].
- [69] T. Piffl et al., *The RAVE survey: the Galactic escape speed and the mass of the Milky Way*, *A&A* **562** (2014) A91 [arXiv:1309.4293].
- [70] E. Del Nobile, G. B. Gelmini, P. Gondolo and J. H. Huh, *Update on light WIMP limits: LUX, lite and light*, *JCAP* **03** (2014) 014 [arXiv:1311.4247].
- [71] K. Hamaguchi, S. P. Liew, T. Moroi, Y. Yamamoto, *Isospin-Violating Dark Matter with Colored Mediators*, arXiv:1403.0324.
- [72] C. Streye et al., *Updated global fits of the cMSSM including the latest LHC SUSY and Higgs searches and XENON100 data*, *JCAP* **1203** (2012) 030 [arXiv:1112.4192]; A. Fowlie, M. Kazana, K. Kowalska, S. Munir, L. Roszkowski, E. Sessolo, S. Trojanowski, and Y.-L. Tsai, *The CMSSM Favoring New Territories: The Impact of New LHC Limits and a 125 GeV Higgs*, *Phys. Rev. D* **86** (2012) 075010 [arXiv:1206.0264]; O. Buchmueller et al., *Higgs and Supersymmetry*, *Eur. Phys. J. C* **72** (2012) 2020 [arXiv:1112.3564].
- [73] K. Paschke et al., *PREX-II Proposal to Jefferson Lab.*, (2012), URL <http://hallaweb.jlab.org/parity/prex/prexII.pdf>.